Microstructure and magnetocaloric effect of melt-spun Ni$_{52}$Mn$_{26}$Ga$_{22}$ ribbon

Z. B. Li, J. L. Sánchez Llamazares, C. F. Sánchez-Valdés, Y. D. Zhang, C. Esling, X. Zhao, and L. Zuo

---

Microstructure and magnetocaloric effect of melt-spun $Ni_{52}Mn_{26}Ga_{22}$ ribbon

Z. B. Li,[1] J. L. Sánchez Llamazares,[2] C. F. Sánchez-Valdés,[3] Y. D. Zhang,[4] C. Esling,[4,a]
X. Zhao,[1] and L. Zuo[1,a]

[1]*Key Laboratory for Anisotropy and Texture of Materials (Ministry of Education), Northeastern University, Shenyang 110819, China*
[2]*Instituto Potosino de Investigación Científica y Tecnológica, Camino a la Presa San José 2055, Col. Lomas 4ª, San Luis Potosí, S.L.P. 78216, Mexico*
[3]*Institut de Ciencia de Materials de Barcelona (CSIC), Campus U.A.B., 08193 Bellaterra, Spain*
[4]*Laboratoire d' Étude des Microstructures et de Mécanique des Matériaux (LEM3), CNRS UMR 7239, Université de Lorraine UDL, 57045 Metz, France*

Microstructural features and magnetocaloric properties of $Ni_{52}Mn_{26}Ga_{22}$ melt-spun ribbons were studied. Results show that there are four types of differently oriented variants of seven-layered modulated (7M) martensite at room temperature, being twin-related one another and clustered in colonies. Due to the coupled magnetic and structural transformations between parent austenite and 7M martensite, the melt-spun ribbons exhibit a significant magnetocaloric effect. At an applied magnetic field of 5 T, an absolute maximum value of the isothermal magnetic entropy change of $11.4 \, J \, kg^{-1} \, K^{-1}$ is achieved with negligible hysteresis losses. © *2012 American Institute of Physics*. [http://dx.doi.org/10.1063/1.4704780]

Heusler-type ferromagnetic shape memory alloys that undergo a martensitic phase transformation may generate large magnetic-field-induced strains because of the strong interaction of their crystallographic structures with an external magnetic field.[1–3] Other than this smart response, they may also exhibit a magnetocaloric effect (MCE) caused by the magnetization change at magnetic phase transition. When such a second-order magnetic phase transition is coupled with the first-order structural phase transformation, i.e., the martensitic transformation, the MCE is maximized and may become giant. For instance, it has been reported that a large magnetic entropy change is linked to the martensite-to-austenite structural phase transition in Ni-Mn-Ga alloys,[4] while it is inverse in Ni-Mn-X (X = In, Sn, Sb) alloys.[5–7] As these alloys possess large MCE and are considerably less expensive than conventional rare-earth-based magnetocaloric alloys with first- or second-order magnetic phase transition, they could be potentially exploited for magnetic refrigeration applications.

It should be noted that the martensitic transformation temperatures of Heusler alloys are sensitive to chemical composition.[8,9] This would enable the co-occurrence of the structural and magnetic transformations (i.e., the magneto-structural transformation)[1,3,4] to maximize the MCE through composition tuning. In general, the magneto-structural transformation can be induced by either a thermal field[4] or a magnetic field.[1,3] However, the magnetic-induced magneto-structural transformation generates a hysteresis loss,[10] which decreases the efficiency of magnetic refrigeration. In this regard, those alloys with the magneto-structural transformations less influenced by magnetic field, such as Ni-Mn-Ga, are considered as more promising and effective magnetic refrigeration materials.

So far, the MCE studies of Heusler alloys have focused mainly on bulk materials. It has been revealed that the alloy with the composition close to $Ni_{55}Mn_{20}Ga_{25}$ can generate significant MCE,[4,11] due to the thermal-induced magneto-structural transformation from ferromagnetic non-modulated (NM) martensite to paramagnetic austenite. However, bulk Heusler alloys appear to be intrinsically brittle and thus difficult to be processed. As an alternative preparation method, the rapid solidification based on melt-spun technique has proven to be an effective single-step processing route for ferromagnetic shape memory alloys like Ni-Mn-Ga, Ni-(Co)-Mn-In, and Ni-Mn-Sn systems,[12–17] which may omit post heat treatment to achieve composition homogeneity. Besides, the melt-spun technique can produce ribbons with appropriate shape for practical devices[18] and highly textured microstructure[19] for property optimization.

In this work, we prepared a polycrystalline Ni-Mn-Ga alloy that possesses the magneto-structural transformation through chemical composition tuning. The precursor alloy with nominal composition of $Ni_{52}Mn_{26}Ga_{22}$ (at. %) was obtained by arc-melting. The as-cast ingot was remelted four times to achieve good composition homogeneity. Using a single copper roller apparatus,[19] the melt-spun ribbons were produced at a wheel-rotating speed of 15 m/s. The direct and reverse martensitic transformation temperatures were measured by differential scanning calorimetry (DSC, TA Q100) in the temperature range from 183 K to 473 K at a heating and cooling rate of 10 K/min. The crystal structure analysis was made with x-ray diffraction (XRD) using Cu-K_α radiation at room temperature. The microstructural characterizations were performed in a field emission gun scanning electron microscope (SEM, Jeol JSM 6500 F) with electron backscatter diffraction (EBSD) system. The magnetization measurements were carried out using the physical property measuring system (PPMS-9T, Quantum Design) equipped with a vibrating sample magnetometer module, where the

---
[a]Authors to whom correspondence should be addressed. Electronic addresses: lzuo@mail.neu.edu.cn and claude.esling@univ-lorraine.fr.

magnetic field was applied along the ribbon length direction (rolling direction) to minimize the demagnetization effect.

Detailed XRD analysis has revealed that the melt-spun ribbons are in a single-phase martensitic state at room temperature and the martensitic phase has a monoclinic incommensurate seven-layered modulated (7M) superstructure (*space group P2/m, No.* 10)[20] with lattice parameters $a = 4.263$ Å, $b = 5.523$ Å, $c = 42.265$ Å, and $\beta = 93.2°$. Fig. 1(a) displays a typical backscattered electron (BSE) image taken on the ribbon plane after electrolytic polishing. It is seen that the martensite appears in plate shape and individual plates are clustered in colonies, where one colony or several colonies outline one original austenite grain. Notably, the melt-spun technique has rendered the austenite grains greatly reduced in size due to an ultra high cooling rate.

Fig. 1(b) shows the room temperature microstructure taken from the cross section perpendicular to the ribbon
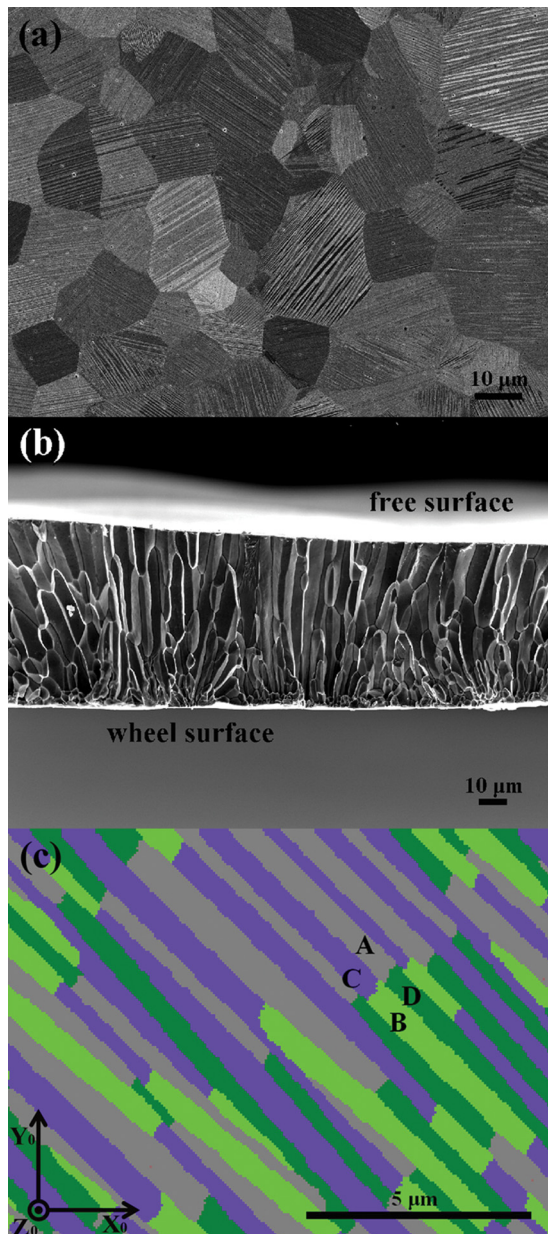

FIG. 1. (a) BSE image of the ribbon plane after electrolytic polishing. (b) Secondary electron image of the cross section. (c) Orientation map showing four types of martensitic variants A, B, C, and D on the ribbon plane.

plane. It is evident that the martensite colonies are in columnar shape, growing approximately along the ribbon plane normal. Moreover, the average austenite grain size at the ribbon surface in contact with the wheel is much smaller than that near the free surface. This morphology should be attributed to the specific heat transfer condition of the melt-spun process.[19]

Fig. 1(c) shows an orientation micrograph of martensite plates taken from the interior of one colony on the ribbon plane (measured at a step size of 0.05 μm), where individual martensite plates are colored according to their crystallographic orientations. It can be seen that the thickness of the martensite plates is greatly reduced with respect to that in the bulk alloy.[21,22] In Fig. 1(c), there are four types of orientation plates (i.e., martensitic variants, designated as A, B, C, and D) distributed alternately within the colony. This is consistent with our previous result on a bulk $Ni_{50}Mn_{30}Ga_{20}$ alloy.[21,22] Furthermore, all the pairs of adjacent variants are twin-related to each other, and their twin relationships can be classified into three categories, i.e., type-I twin for A and C (or B and D), type-II twin for A and B (or C and D) and compound twin for A and D (or B and C). The complete twinning elements for the three categories of twins are shown in Table I.

Fig. 2(a) presents the temperature dependence of magnetization $M(T)$ under a magnetic field of 5 mT and the DSC curves of the melt-spun ribbon sample during heating and cooling. The thermomagnetic measurements were performed using the following thermal protocol: the sample was first heated to 400 K with an applied low field of 5 mT; then the $M(T)$ values were taken during field-cooling (FC) from 400 K to 10 K and subsequent field-heating (FH) to 400 K, with the temperature intervals of 1.5 K (400 K–260 K) and 5 K (255 K–10 K). The temperature sweep rate was 1 K/min and the approach mode to each temperature was "no overshot" to ensure the measurement accuracy. In both the FH and FC processes, a sudden change of the magnetization has occurred around 350 K, which should be attributed to the paramagnetic–ferromagnetic transition. The Curie temperatures (T_C) on cooling and heating were determined to be 350 K and 351 K, respectively. The thermal hysteresis of the magnetic phase transition is about 1 K, which is within the measurement uncertainty and in practice negligible. Moreover, according to the heating and cooling DSC curves, the direct and reverse martensitic transformation temperatures were determined to be 346 K (M_s), 332 K (M_f), 341 K (A_s), and 354 K (A_f). The thermal hysteresis (A_f - M_s) of the martensitic transformation is 8 K. Note that the magnetic

TABLE I. Twinning elements of incommensurate 7M martensite in $Ni_{52}Mn_{26}Ga_{22}$ ribbons.

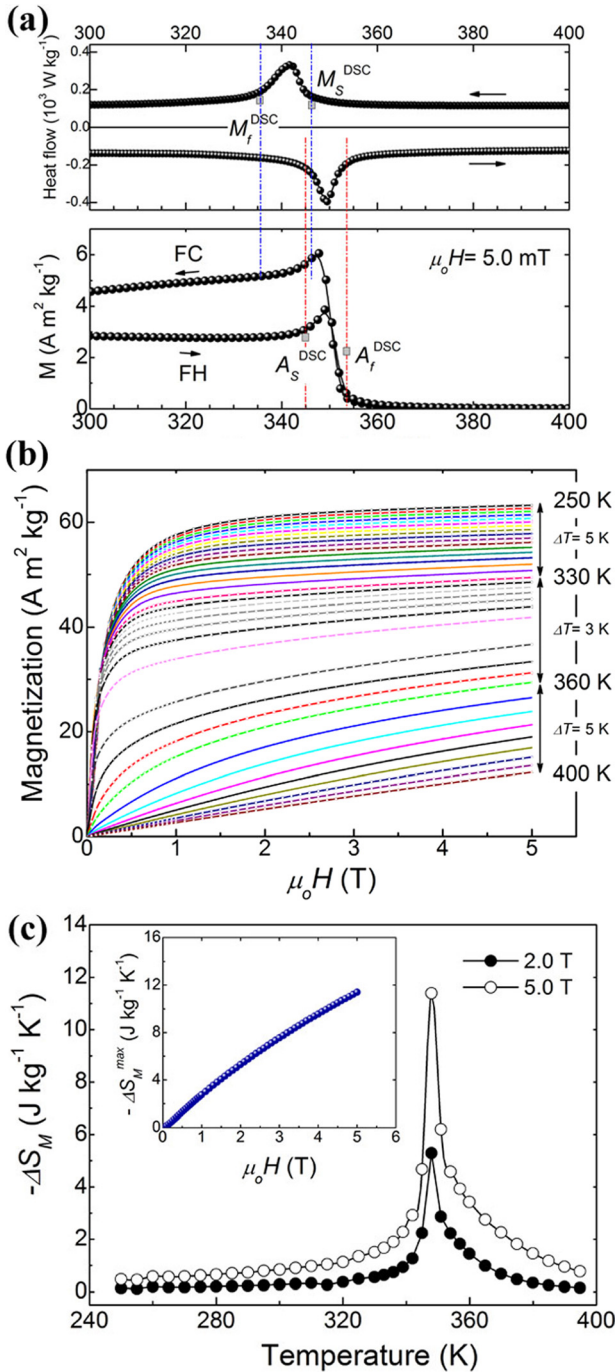| Elements	Type I (A:C/B:D)	Type II (A:B/C:D)	Compound (A:D/B:C)
K_1	$(1\ \bar{2}\ \overline{10})$	$(1.0821\ \bar{2}\ \overline{9.1786})$	$(1\ 0\ 10)$
K_2	$(\overline{1.0821}\ \bar{2}\ 9.1786)$	$(\bar{1}\ \bar{2}\ 10)$	$(\bar{1}\ 0\ 10)$
η_1	$[\overline{10.7367}\ \overline{10}\ 0.9263]$	$[\overline{10}\ \overline{10}\ 1]$	$[\overline{10}\ 0\ 1]$
η_2	$[10\ \overline{10}\ \bar{1}]$	$[10.7367\ \overline{10}\ \overline{0.9263}]$	$[10\ 0\ 1]$
P	$(1\ \overline{0.076}\ 10.7649)$	$(1\ 0.076\ 10.7649)$	$(0\ 1\ 0)$
S	0.2218	0.2218	0.0172

FIG. 2. (a) Heating and cooling DSC curves (upper) and thermal dependence of magnetization $M(T)$ at 5 mT (lower). The vertical dashed lines correlate the start and finish phase transition temperatures (determined from the DSC scans) with the features of the low-field $M(T)$ curves. (b) Isothermal magnetization curves $M(H)$ in the temperature range from 250 to 400 K. (c) Temperature dependence of magnetic entropy change $\Delta S_M(T)$ at a magnetic field of 2 T and 5 T. The inset shows the field dependence of absolute maximum magnetic entropy change.

transformation temperatures derived from the thermomagnetic measurements are just located within the martensitic transformation temperature range determined by the DSC measurements. This could be a reason accounting for the fact that the structural transformation temperatures are not well distinguished in the $M(T)$ curves (in Fig. 2(a), the vertical dashed lines were traced to help facilitate the locations of the structural transition temperatures with respect to the changes

in the $M(T)$ curves). By comparing the $M(T)$ curves with the DSC curves, one can confirm that the magnetic transformation and the structural transformation occurred almost simultaneously.

In fact, the DSC signals are sensitive to the heat flow variations when heating or cooling a sample and the phase transitions are associated with exothermic or endothermic processes, which allow the determination of the start and finish transition temperatures. In contrast, the magnetic moment signals of the sample across the structural phase transition depend on how the magnetic exchange interactions change upon the inter-atomic distances of magnetically coupled atoms in either martensite or austenite phase. With a careful examination on the heating and cooling pathways shown in Fig. 2(a), it is found that during heating a rise of magnetization occurred just at the A_s^{DSC} in the $M(T)$ curve (which is also accompanied by a change in the slope of the curve) and the A_f^{DSC} lay in the paramagnetic region, while on cooling a drop of magnetization took place just at the M_s^{DSC} in the $M(T)$ curve and the M_f^{DSC} lay in the ferromagnetic region. Therefore, in the present case where the structural and magnetic transitions were coupled, the characteristic structural phase transformation temperatures (A_s, A_f, M_s, and M_f), as well as the thermal hysteresis ($A_f - M_s$), were well determined from the DSC curves but not from the low-field magnetization measurements. As the ferromagnetic martensite is directly transformed into the paramagnetic austenite during heating, large changes in the magnetic entropy should be expected in the vicinity of the magneto-structural transition.

In order to characterize the magnetocaloric effect of the ribbons, sets of magnetization isotherms $M(H)$ were measured from 250 K to 400 K (with the step increments ΔT) up to a maximum applied magnetic field of $\mu_o H_{max} = 5$ T (Fig. 2(b)). The thermal protocol followed to measure each $M(H)$ curve around the magneto-structural transformation was carefully chosen for a correct determination of the temperature dependence of magnetic entropy change across the martensite-to-austenite transition. It is evident that the magnetization decreases with increasing temperature under a given magnetic field. The isothermal magnetic entropy change ΔS_M was derived from the measured isothermal magnetization curves by numerical integration of the Maxwell relation[23], i.e., $\Delta S_M(T,H) = \mu_0 \int_0^H (\partial M/\partial T)_H dH$. Fig. 2(c) shows the calculated ΔS_M values as a function of temperature under a magnetic field of 2 T and 5 T. A sharp peak was found at 348 K, with an absolute maximum magnetic entropy change $|\Delta S_M^{max}|$ of 5.3 J kg^{-1} K^{-1} at 2 T and 11.4 J kg^{-1} K^{-1} at 5 T. The $|\Delta S_M^{max}|$ vs H curve is displayed as the inset in Fig. 2(c). The significant absolute maximum values of the isothermal magnetic entropy change should be ascribed to the coupled nature of the magneto-structural transformation.

An important parameter to evaluate the magnetocaloric properties of a material refers to the hysteresis loss around the phase transition,[10,12] since the hysteresis losses reduce the refrigeration capacity of the refrigerant cycle. Fig. 3(a) shows the field-up and field-down magnetization $(M(H))$ curves up to $\mu_o H_{max} = 5$ T recorded at different temperatures (with a step increment of $\Delta T = 3$ K), where the martensite-to-austenite phase transition was thermally induced. The hysteresis loss values were obtained by calculating the areas
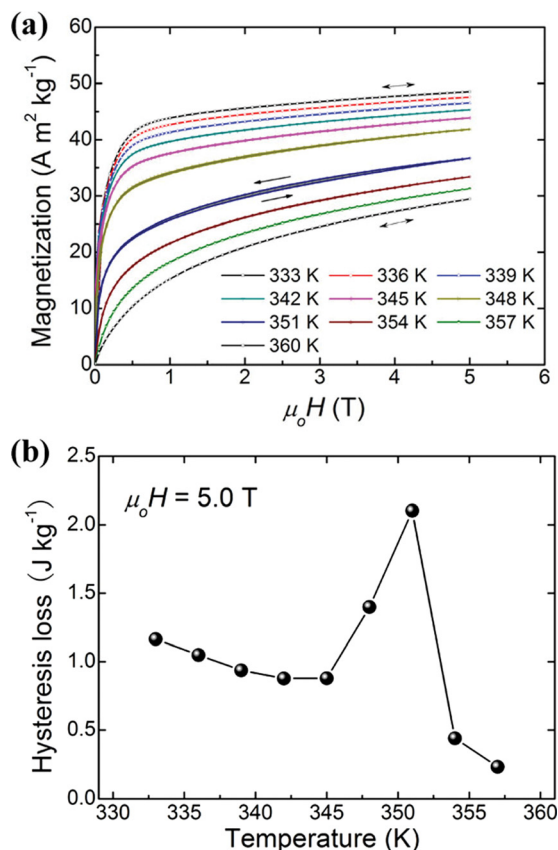
FIG. 3. (a) Field-up and field-down isothermal magnetization curves. (b) Hysteresis losses at 5 T as a function of temperature across the martensite-to-austenite transformation.

enclosed between the field-up and field-down $M(H)$ curves. Fig. 3(b) presents the hysteresis losses at 5 T as a function of temperature. It is worth mentioning that the present alloy does not show significant hysteresis losses. The maximum loss is about 2.1 J/kg at 351 K.

In summary, the microstructural features, magnetostructural transformation, and magnetocaloric effect of $Ni_{52}Mn_{26}Ga_{22}$ melt-spun ribbons were studied. EBSD examinations revealed that the room temperature microstructures consist of incommensurate 7M modulated martensite, where four types of variants are twin-related one another and clustered in colonies. The co-occurrence of the structural and magnetic phase transformations from the ferromagnetic 7M martensite to the paramagnetic austenite was evidenced by DSC and thermomagnetic measurements, producing large isothermal magnetic entropy change (with the absolute maximum value of 11.4 J kg^{-1} K^{-1}) and negligible hysteresis loss (with the maximum value of 2.1 J/kg) under 5 T. This makes the melt-spun ribbons of interest as a potential dual-functional material, i.e., magnetic shape memory and magnetic refrigeration.

[1]R. Kainuma, Y. Imano, W. Ito, Y. Sutou, H. Morito, S. Okamoto, K. Oikawa, A. Fujita, T. Kanomata, and K. Ishida, Nature (London) **439**, 957 (2006).
[2]S. J. Murray, M. Marioni, S. M. Allen, R. C. O'Handley, and T. A. Lograsso, Appl. Phys. Lett. **77**, 886 (2000).
[3]R. Kainuma, Y. Imano, W. Ito, H. Morito, Y. Sutou, K. Oikawa, A. Fujita, K. Ishida, S. Okamoto, O. Kitakami, and T. Kanomata, Appl. Phys. Lett. **88**, 129513 (2006).
[4]M. Pasquale, C. P. Sasso, L. H. Lewis, L. Giudici, T. Lograsso, and D. Schlagel, Phys. Rev. B **72**, 094435 (2005).
[5]X. Moya, L. Mañosa, A. Planes, S. Aksoy, M. Acet, E. F. Wassermann, and T. Krenke, Phys. Rev. B **75**, 184412 (2007).
[6]I. Dubenko, M. Khan, A. K. Pathak, B. R. Gautam, S. Stadler, and N. Ali, J. Magn. Magn. Mater. **321**, 754 (2009).
[7]W. J. Feng, L. Zuo, Y. B. Li, Y. D. Wang, M. Gao, and G. L. Fang, Mater. Sci. Eng., B **176**, 621 (2011).
[8]V. A. Chernenko, Scr. Mater. **40**, 523 (1999).
[9]X. Moya, L. Mañosa, A. Planes, T. Krenke, M. Acet, and E. F. Wassermann, Mater. Sci. Eng., A **438–440**, 911 (2006).
[10]P. J. Shamberger and F. S. Ohuchi, Phys. Rev. B **79**, 144407 (2009).
[11]V. V. Khovailo, T. Takagi, J. Tani, R. Z. Levitin, A. A. Cherechukin, M. Matsumoto, and R. Note, Phys. Rev. B **65**, 092410 (2002).
[12]B. Hernando, J. L. Sánchez Llamazares, V. M. Prida, D. Baldomir, D. Serantes, M. Ilyn, and J. González, Appl. Phys. Lett. **94**, 222502 (2009).
[13]N. V. Rama Rao, R. Gopalan, M. Manivel Raja, J. Arout Chelvane, B. Majumdar, and V. Chandrasekaran, Scr. Mater. **56**, 405 (2007).
[14]J. Liu, T. G. Woodcock, N. Scheerbaum, and O. Gutfleisch, Acta Mater. **57**, 4911 (2009).
[15]B. Hernando, J. L. Sánchez Llamazares, J. D. Santos, Ll. Escoda, J. J. Suñol, R. Varga, D. Baldomir, and D. Serantes, Appl. Phys. Lett. **92**, 042504 (2008).
[16]J. L. Sánchez Llamazares, T. Sanchez, J. D. Santos, M. J. Pérez, M. L. Sanchez, B. Hernando, Ll. Escoda, J. J. Suñol, and R. Varga, Appl. Phys. Lett. **92**, 012513 (2008).
[17]J. L. Sánchez Llamazares, B. Hernando, C. García, J. González, Ll. Escoda, and J. J. Suñol, J. Phys. D: Appl. Phys. **42**, 045002 (2009).
[18]Y. Tong and Y. Liu, J. Alloys Compd. **449**, 152 (2008).
[19]Z. B. Li, J. J. Wang, Y. D. Zhang, K. Z. He, X. Zhao, L. Zuo, G. Hofer, and C. Esling, Adv. Eng. Mater. **12**, 1024 (2010).
[20]L. Righi, F. Albertini, E. Villa, A. Paoluzi, G. Calestani, V. Chernenko, S. Besseghini, C. Ritter, and F. Passaretti, Acta Mater. **56**, 4529 (2008).
[21]Z. B. Li, Y. D. Zhang, C. Esling, X. Zhao, Y. D. Wang, and L. Zuo, J. Appl. Cryst. **43**, 617 (2010).
[22]Z. B. Li, Y. D. Zhang, C. Esling, X. Zhao, and L. Zuo, Acta Mater. **59**, 2762 (2011).
[23]A. M. Tishin and Y. I. Spichkin, *The Magnetocaloric Effect and Its Applications* (Institute of Physics Publishing, Bristol, 2003).